Electronic Supplementary Material (ESI) for Chemical Communications.

Electronic Supplementary Information (ESI)

Dual Active Sites in Triazine-Based Covalent Organic Polymeric Framework Promoting Oxygen Reduction Reaction

*Tribani Boruah, [†a] Sabuj Kanti Das, [†a] Greesh Kumar, [†a] Saptarsi Mondal, [b] and Ramendra Sundar Dey**

[a]*Institute of Nano Science and Technology, Sector-81, Mohali, 140306, Punjab, India*

[b]*Center for Molecular Spectroscopy and Dynamics, Institute of Basic Science (IBS), Seoul 02841, Republic of Korea.*

**Corresponding author. E-mail: rsdey@inst.ac.in*

†These authors contributed equally.

Section S1	Material, instrumentations and experimental part.
Figure S1	^{1}H-NMR spectrum of DFP.
Figure S2	^{1}H-NMR spectrum of TAPT.
Figure S3	Schematic representation of synthesis of Trz-COP
Figure S4	Fe-SEM image of Trz-COP before and after base treatment
Figure S5	Full XPS survey of Trz-COP, C1s ,N1s spectra after stability , O1s both before and after stability,
Table S1	Elemental analysis of Trz-COP catalyst obtained from XPS analysis.
Table S2	Peak table of C1s XPS spectra of Trz-COP before stability
Table S3	Assigning FTIR peak positions for Trz-COP
Figure S6	TGA plot of Trz-COP.
Figure S7	(a) PXRD (b)FTIR spectra of TPA-COF (control sample)
Figure S8	Cyclic voltammetry (CV) analysis of Trz-COP catalyst in the presence of Ar and O_2 saturated 0.1 M KOH electrolyte solution.
Figure S9	Linear sweep voltammetry (LSV) polarization curve of Trz-COP and Pt/C catalyst at 1600 rpm in O2 saturated 0.1 M KOH electrolyte solution.
Figure S10	Electrochemical impedance spectroscopy (EIS) analysis of Trz-COP catalysts Nyquist plot and equivalent circuit.
Figure S11	Linear sweep voltammetry (LSV) polarization curve of Trz-COP catalyst at all

	rotation speeds 625 to 4900 rpm in O_2 saturated 0.1 M KOH electrolyte solution.
Figure S12	Linear sweep voltammetry (LSV) polarization curve of Trz-COP catalyst at 1600 rpm in O_2 saturated 0.1 M KOH electrolyte solution with disk and ring current.
Figure S13	Linear sweep voltammetry polarization curve before and after stability of Trz-COP catalyst.
Figure S14	Chronoamperometry analysis of Trz-COP and Pt/C catalyst with 1M CH_3OH for checking methanol tolerance.
Figure S15	CV analysis Trz-COP catalyst with 1M CH_3OH and without CH_3OH in O_2 saturated KOH electrolyte.
Figure S16	CV analysis of Pt/C catalyst with 1M CH_3OH and without CH_3OH in O_2 saturated KOH
Figure S17	(a) FTIR (b) PXRD spectra of Trz-COP after stability
Section S2	DFT Study – results and discussion
Figure S18	1:1 complex of Trz-COP with dual binding sites interact with O_2, optimized at B3LYP/6-31+G (D,P) level of theory. The bond length of the adsorbed O_2 is mentioned in Å for each complex showing that O_2 bond length in these complexes has increased compared to that of the pure O_2.
Table S4	The zero-point vibrational energy (ZPVE) corrected complexation energy, O=O bond length (Å), type of the noncovalent interaction, electrostatic potential-derived atomic charges (a.u.), electron density [ρ(r)], Laplacian of electron density [L(r)] and ellipticity (ε) at the (3, -1) bond critical point representing the respective noncovalent interaction of various 1:1 complex of Trz-COP form with O_2.
Section S3	DFT -Methodology

Figure S19	ESP-derived atomic charges of (a) Trz-COP and its 1:1 complex with O_2, (b) A1, and (c) A2.
Figure S20	Molecular electron density map of the 1:1 complexes of O_2 with Trz-COP (A1, A2) calculated at B3LYP/6-31+G (D, P) level of theory. Green and red spheres represent bond critical points (BCP) and ring critical points (RCP). The presence of BCP between the phenyl ring carbon along with nitrogen atom (from –C-N of imine and triazine) and O_2 molecule as well as terminal carbon/nitrogen atom and O_2, along with their corresponding topological parameters, suggests weak non-covalent interactions between them.
Figure S21	Mechanistic pathway for ORR

Section S1

Experimental section

Chemicals: This analysis utilized phosphorous oxychloride (153.33 g mol^{-1}), phloroglucinol (126.11g mol^{-1}), and hexamine (140.18 $gmol^{-1}$) were supplied by Sigma-Aldrich, India. Trifluoromethanesulfonic acid, potassium hydroxide (KOH), as well as 4-aminobenzonitrile (M =118.14), 1,4-dioxane, mesitylene, and other organic solvents were utilized as obtained from Spectro-chem, India, with no further purification.

Instrumental techniques A Bruker AXS D-8 Advanced SWAX diffractometer was employed to obtained the powder X-diffration (PXRD) pattern via utilising Cu-K$\boldsymbol{\alpha}$($\boldsymbol{\lambda}$= 1.5406 Å) source of radiation. The Fourier-transform infrared spectroscopy (FTIR) technique was used to analyze the bonding connectivity of the as-synthesized material using a Perkin Elmer Spectrum 100 spectrophotometer. For liquid and solid-state, NMR have been recorded using 400 MHz Bruker-Advance II. Further to confirm the presences of different types N, O, C XPS analysis has been performed using Thermo Fisher Instrument with Cu-kα as source of radiation. While, BET surface area analysis data were obtained from a surface area/porosity analyzer (Quantachrome Autosorb-iQ, USA). Additionally, to determine the pore size distribution of the generated N_2 adsorption-isotherm, Non-Local Density Functional Theory (NLDFT) was utilized. Moreover, to determine the thermal stability of the as-synthesized material, Thermo-gravimetric analysis was carried out in a Mettler Toledo TGA/DTA 851e TA-SDT Q-600 instrument. Field emission scanning electron microscopy (FESEM) images of the material were collected from a JEOL JEM 6700 instrument.

Synthesis of Diformylphloroglucinol (DFP) To perform the diformylation reaction of phloroglucinol, Vilsmeier-reagent was obtained by adding 3.67 g (0.024 mol) of phosphorous oxychloride ($POCl_3$) to 1.75 g (0.024 mol) of anhydrous DMF solvent and stirring at room temperature (298 K) for 30 mins, maintaining the inert atmospheric conditions.[1] Anhydrous phloroglucinol (1.0 g, 0.008 mmol) in dioxane (10 mL) solvent was then gradually added to the reaction mixture under an inert N_2 environment and proceed the reaction in stirring conditions at 315K for 12 hours. A yellow-amorphous solid was formed which was then cooled to zero degrees Celsius. Further, stirring was continued for another four hours at room temperature after the addition of ice-cooled water (40 mL) to the solid product. A cream-colored precipitate is generated throughout the process. The precipitate was then filtered off and washed with plenty of distilled water (DI) to eradicate any remnant residues. In the next step, the solid product was solubilized in a relatively minimal volume of DI water and subsequently extracted with ethyl-acetate 2-3 times. After two times brine solution (saturated NaCl-H_2O) treatment, the organic layer was dried using anhydrous $NaSO_4$, as well as the ethyl acetate was removed using rotavapor to achieve the desired product. The resultant as-synthesized monomer (DFP) was dried for approximately 16 hours under vacuum at 360 K to obtain a yield of 1.27 g of the final product, 7.0 mmol, 88%.

^{1}H-NMR (400 MHz, DMSO-d_6) δ ppm 5.97 (s, 1 H, Ar-H), 10.08 (s, 2 H, CHO), 12.56 (Br. S., 2 H, OH), 13.59 (Br. S., 1 H, OH). ^{1}H-NMR spectrum is shown in Figure S1.

Synthesis of 1, 3, 5-Tris-(4-aminophenyl) triazine (TAPT)

The TAPT monomeric unit was synthesized separately via carrying out the reaction between 4-aminobenzonitrile and super-acids as catalyst. As per the literature reported synthesized procedure[2], the desired reaction was carried out in an ice-bath where 4-aminobenzonitrile (1.544g,13.076mmol) was taken in a round bottom (RB) flask accompanied by the drop-wise addition of *triflic acid* (4ml, 44.4 mmol) while maintaining the temperature at 0^{o}C. Then the resultant reaction mixture was allowed to stir for about 24 hours under nitrogen atmosphere at RT Afterwards, ice-cold distilled water (20 ml) was added to the finally obtained slurry and followed by the addition of 2 M o a basic solution (NaOH) to neutralize the resultant slurry at pH-7. Furthermore, the conventional filtration technique was employed to obtain the final yellow-colored solid product, and then the remaining basic residue (NaOH) was removed by washing with DI water approximately 5 times. The final purified product was further characterized using ^{l}H NMR spectroscopy. The yield of the product was~ 93 %.

^{1}H-NMR (400 MHz, DMSO-d^6) δ ppm 8.42 (d, 6 H, Ar-H), 6.76 (d, 6 H, Ar-H), 5.95 (s, 6H, -NH_2).

^{1}H-NMR spectrum is shown in Figure S2

Synthesis of porous organic polymer (Trz-COP).

A Schiff-base condensation polymerization reaction was employed to synthesize the desired porous polymeric framework (Trz-COP). 2,4,6-trihydroxyisophthalaldehyde of 0.055g (0.3mmmol) and TAPT of 0.071g (0.2mmol) was taken in a Schlenk tube along with 4 mL of the dioxane-mesitylene solvent mixture in a 9:1 ratio, followed by the addition of 6(M) CH_3COOH as a catalyst. Then, the resultant reaction mixture was allowed to sonicate for 10 min, and degassing was carried out by using Liq. N_2 in 3 freeze-pump-thaw cycles subsequently. Afterward, the reaction mixture was allowed to be kept in an oil bath for 4 days at 120 ^oC. Finally, the deep red colored desired product was separated by filtration, which was further continued to be washed with dioxane, methanol, tetrahydrofuran (THF), H_2O, and CH_3COCH_3. The powder sample has been dried at 120^o C under vacuum conditions for 12 hours to achieve guest-free Trz-COP material (70 % isolated yield).

Control experiments

Synthesis of TPA-COFs

TPA-COFs material was prepared by a Schiff base polycondensation method via solvothermal approach where, tris(4-aminophenyl) amine 0.05mmol, 0.05 mmol tris(4-formylphenyl) amine, o-dichlorobenzene (5ml) , ethanol (5ml), 3 M acetic acid were added in a beaker and allowed to sonicated for 45 min to obtained a homogeneous mixture which was then transferred to an autoclave , under N_2 gas purging and kept in an oven at 120°C for 72 hours. The obtained product was centrifuged and washed with DMF, acetone, and then ethanol. Sample was allowed to dried in a vacuum oven at 60°C. The final product was obtained with a yield of 78%.

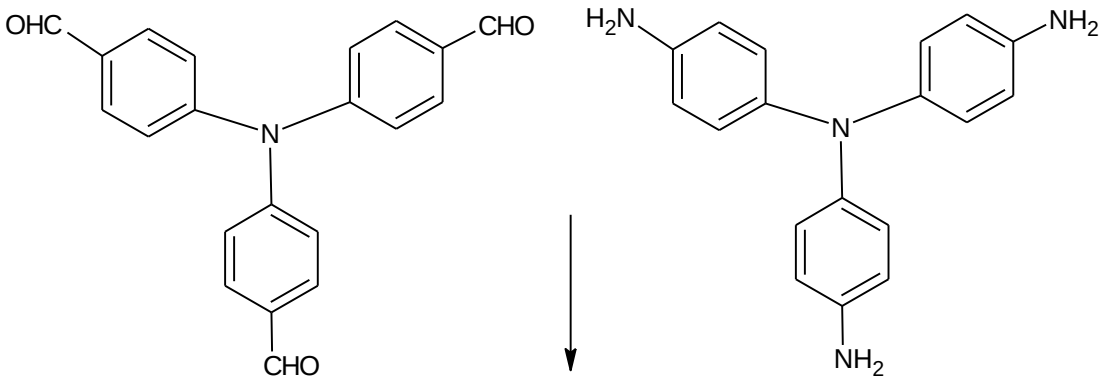

tris(4-aminophenyl) amine tris(4-aminophenyl) amine

TPA-COFs

Schematic representation of synthesis of TPA-COF

Electrochemical measurements CHI 760E and Metrohm Multi Auto-lab/M204 electrochemical work-station consisting of three-electrode cell namely working electrode [RDE (rotating disk electrode) dia-3mm, RRDE (rotating ring disk electrode) dia-5mm], reference electrode (3M-KCl, Ag/AgCl) and counter electrode (graphite rod dia-10 mm) was used to record the electrochemical data for the as-synthesized porous polymeric network. The catalyst ink was prepared by using 5 mg of catalyst in water and isopropanol (1:1) and sonicating for 30 minutes. For comparison, Pt/C ink was prepared in ethanol and DI water containing Nafion (5%) solution, which was dispersed by ultrasonication for 30 min. Before drop-casting, the catalyst on the electrodes, the glassy carbon, RDE, and RRDE electrodes were polished by using 1, 0.3, and 0.05 µm alumina powder (Al_2O_3) and washed with DI water ultrasonically. All the catalysts were drop-casted on the electrodes to maintain a mass loading of 0.65 mg cm^{-2}. Moreover, the following experiments have been performed after 30 minutes of oxygen gas purging in 0.1 M KOH to record the cyclic voltammetry (CV), llinear sweep voltammetry (LSV), chronoamperometry, and electrochemical impedance spectroscopy (EIS), respectively.

The obtained potentials were calibrated to RHE (reversible hydrogen electrode) using the equation given below.[3]

$$\boldsymbol{E(RHE)\ (V) = E\_(Ag/AgCl)\ \ (3\ M\ KCl)\ V + \ (0.058\ \times\ pH)\ \ V + \ 0.210\ V} \qquad (1)$$

The number of electron transfer (n) per O_2 participate in ORR can be determined by Koutecky-Levich (K-L) equation-

$$\frac{1}{J} = \frac{1}{J_L} + \frac{1}{J_K} = \frac{1}{B\omega^{\frac{1}{2}}} + \frac{1}{J_K} \qquad (2)$$

J is the measured current density, J_K (kinetic current density) and J_L (diffusion-limiting current density), ω is the angular velocity of the disk (ω = 2πN, linear rotation speed (N), n is the overall number of electrons transferred in ORR, Faraday constant (F = 96485 C mol^{-1}), ϑ is the kinematic viscosity of the electrolyte, C_0 is the bulk concentration of O_2, k is the electron transfer rate constant diffusion coefficient, and (D_0) of O_2 in electrolyte solution. The *B* and J_K values can be resolved from the Koutecky-Levich (K-L) plots based on the Levich equation below.

$$B = 0.62nFC_0 D_0^{2/3} \vartheta^{-1/6} \qquad (3)$$

$J_K = nFkC_0$ (4)

For the ORR analysis, the total no. of electrons (n) participating in the reaction was calculated by using equation (5) while, the percentage of hydrogen peroxide (%H_2O_2) generation was evaluated by using equation (6),

$$n = 4 \times \frac{I_D}{I_D + \frac{I_R}{N}} \quad (5)$$

$$\%H_2O_2 = 200 \times \frac{\frac{I_R}{N}}{\frac{I_R}{N} + I_D} \quad (6)$$

I_D and I_R respectively denote disk and ring current, whereas, N=0.249 accounts to the collection proficiency of Pt-ring.

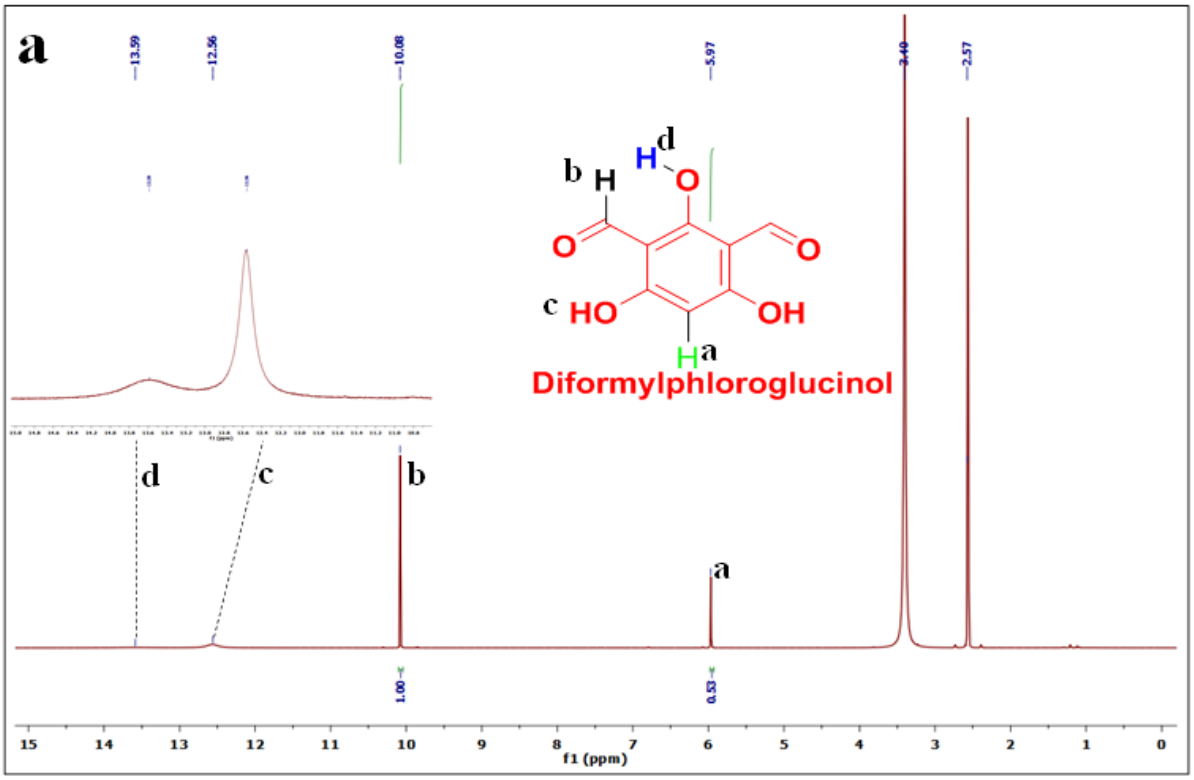

Figure S1. ^{1}H-NMR spectrum of DFP

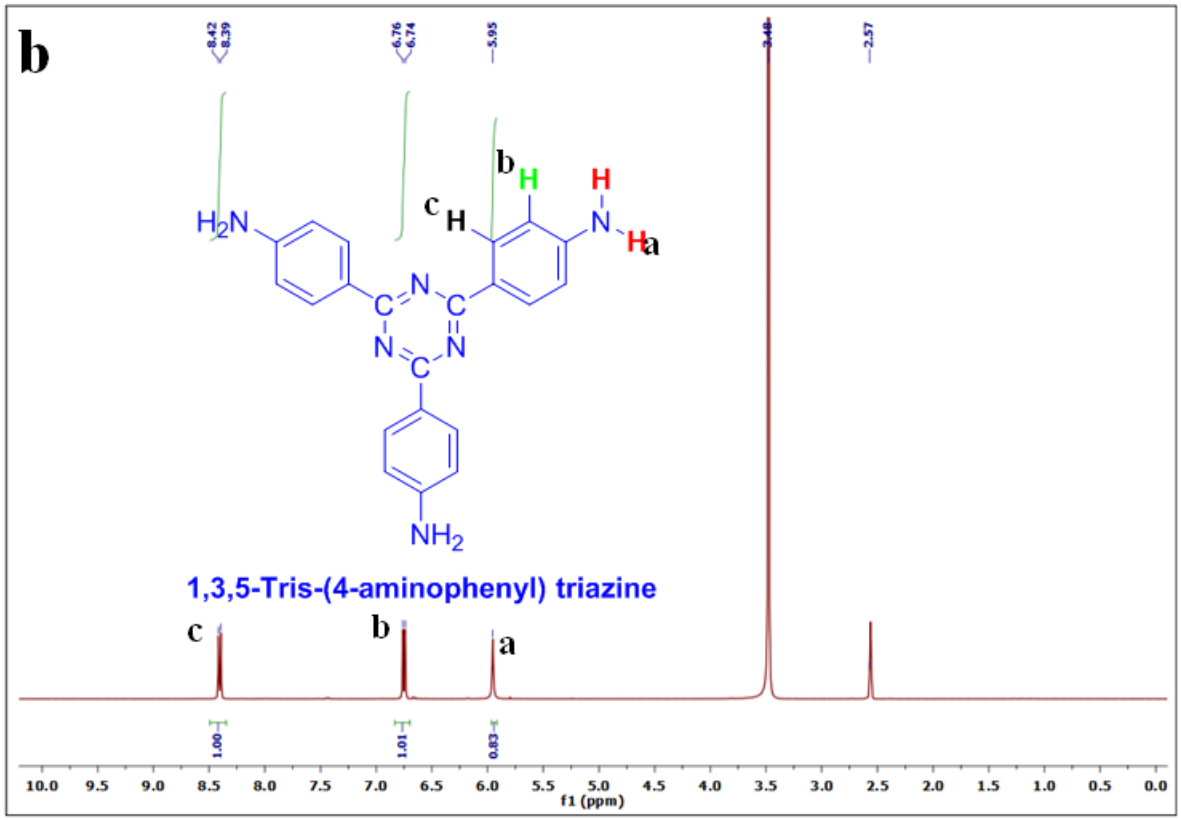

Figure S2. ^{1}H-NMR spectrum of TAPT

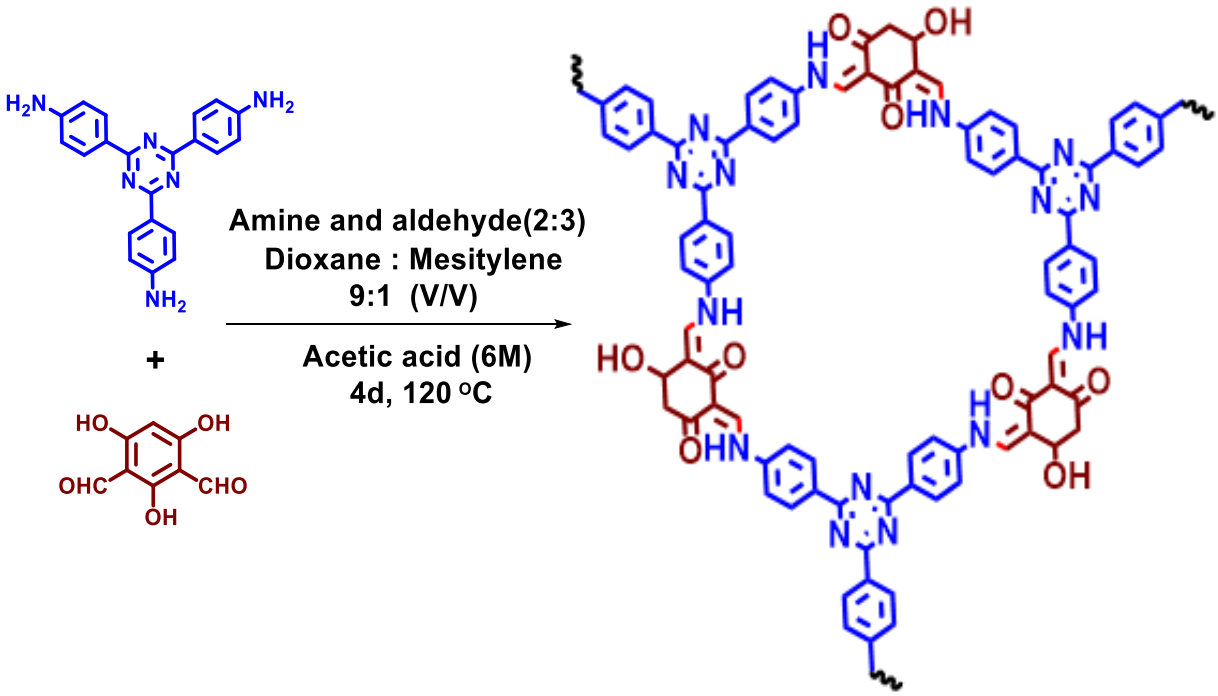

Figure S3 Schematic representation of synthesis of Trz-COP

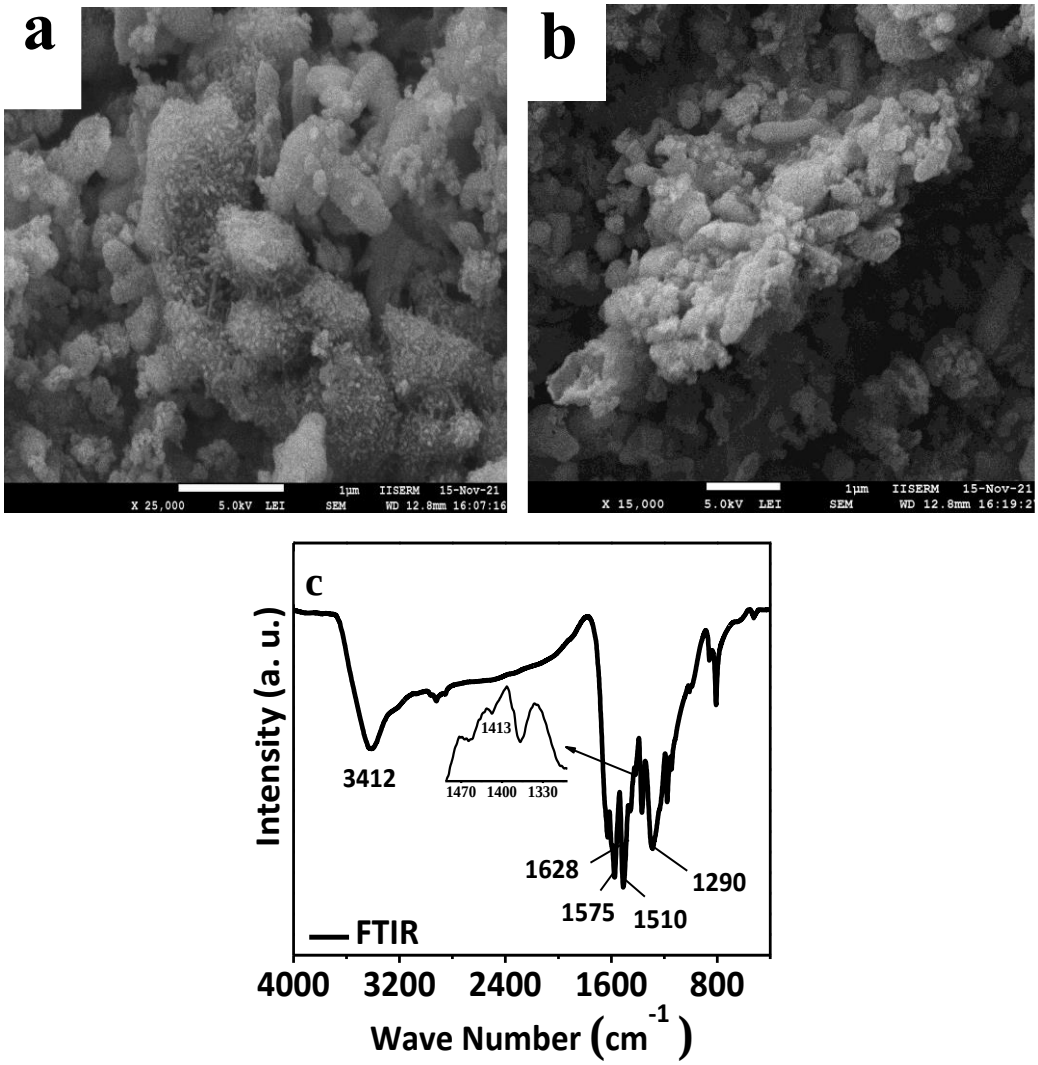

Figure S4. FESEM image of Trz-COP- (a) before and (b) after base *treatment* (c)FTIR spectrum Trz-COP

The presence of C=C with the co-existence of keto-enol tautomerization was indicated by the sharp IR band at 1575 cm^{-1}, while, 1628 cm^{-1} and 1290 cm^{-1} absorption bands confirmed the existence of functionalized alpha-beta unsaturated ketone and -C-N linkage respectively.

In ^{13}C-NMR, the appearance of strong resonance peaks around 131.2, 120.3, 113.8, 107.2 and 100.2 ppm indicate the existences of different aromatic C-atoms present in the Trz-COP polymeric network (C atoms marked as 6,7,8,9 and 10 respectively

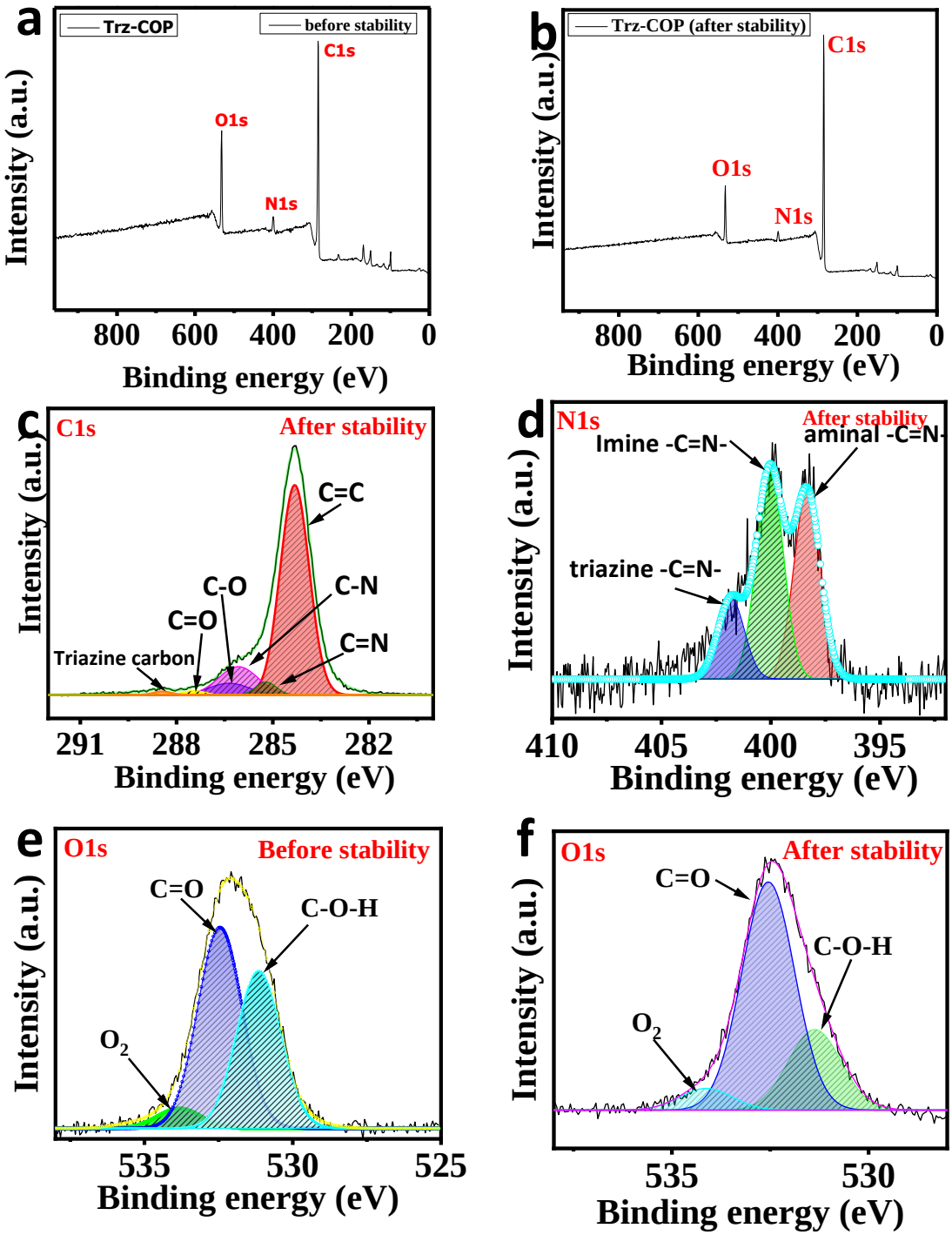

Figure S5. (a,b) Full XPS survey of Trz-COP both before and after stability, (c,d) C1s ,N1s spectra after stability (e,f) O1s spectra before and after stability.

Obtained XPS analysis confirmed the presences of N, O, C with appropriate elemental analysis percentage, presented in the table 1 given below. In the O1S spectra peaks at 530.54ev, 531.9 ev, 533.09 ev and 534.8 ev clearly confirmed the presences of C-O, -C-OH,-C=O and surface absorbed O_2 respectively within the polymeric network.

Table S1. Elemental analysis of Trz-COP catalyst obtained from XPS analysis

Before stability		
Elements	**Binding energy (eV)**	**Atomic (%)**
Carbon (C)	285.08	84.78
Nitrogen (N)	400.08	5.34
Oxygen (O)	532.08	9.88
After stability		
Elements	**Binding energy (eV)**	**Atomic (%)**
Carbon (C)	285.08	86.05
Nitrogen (N)	399.08	5.04
Oxygen (O)	532.08	8.90

Functional groups	Binding energy (eV)
Triazine carbon	288.4
C=O	287.5
C-O	286.5
C-N	286.03
C=N	285.2
C=C	284.3

Table S2. C1s XPS spectra of Trz-COP before stability.

Functional groups	Wave number (cm^{-1})
-N-H stretch	3412
Alpha-beta-unsaturated ketone	1628
C=C stretching	1575
Triazine ring(stretching)	1508
C=C (aromatic stretching)/ -N-H bending	1454
-O-H	1413
Triazine ring (bending)	1359
-C=N-	1290
C-N stretching	1010
Breathing mode of vibration of triazine units	808

Table S3. Assigning FTIR peak positions for Trz-COP

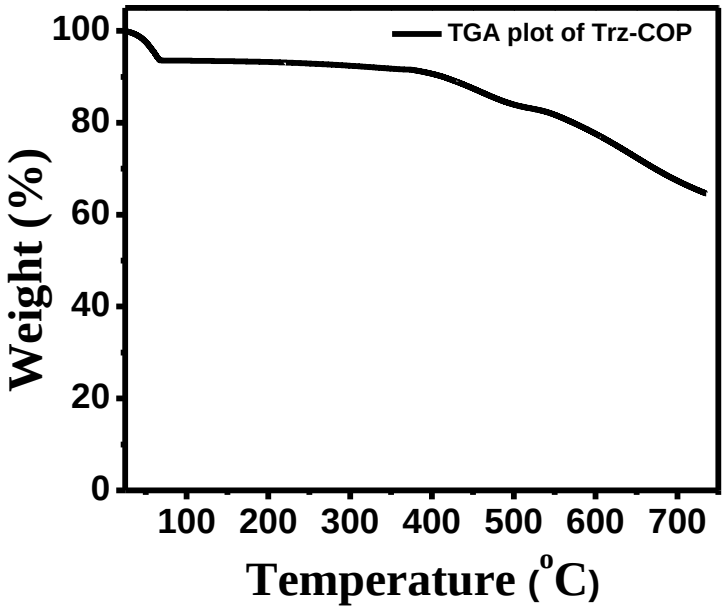

Figure S6. TGA plot of Trz-COP

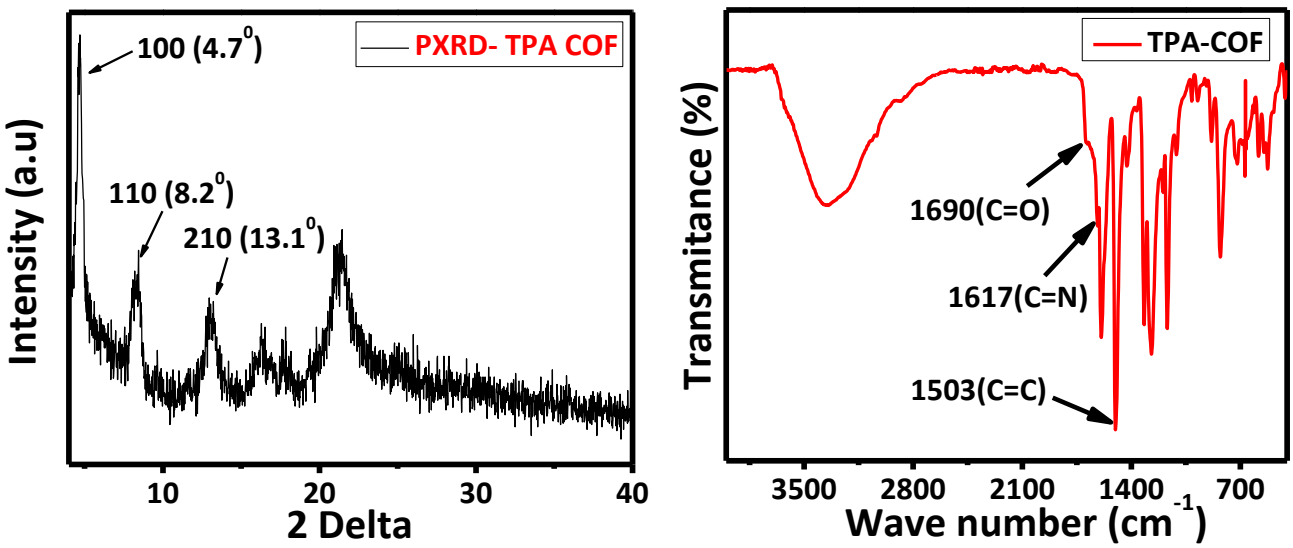

Figure S7. (a) PXRD (b)FTIR spectra of TPA-COF

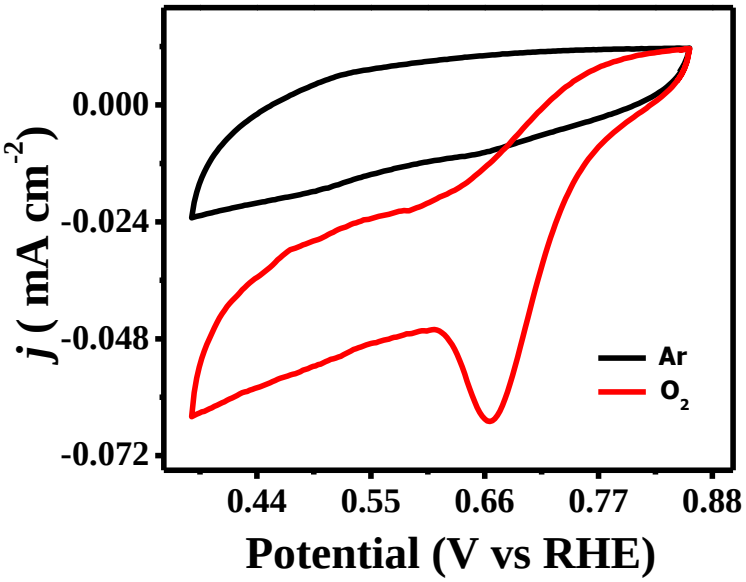

Figure S8. Cyclic voltammetry (CV) analysis of Trz-COP catalyst in the presence of Ar and O_2 saturated 0.1 M KOH electrolyte solution

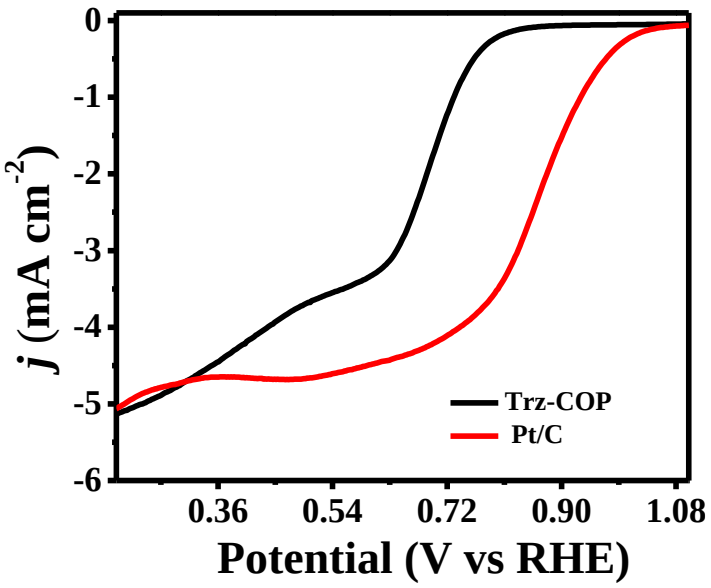

Figure S9. Linear sweep voltammetry (LSV) polarization curve of Trz-COP and Pt/C catalyst at 1600 rpm in O_2 saturated 0.1 M KOH electrolyte solution

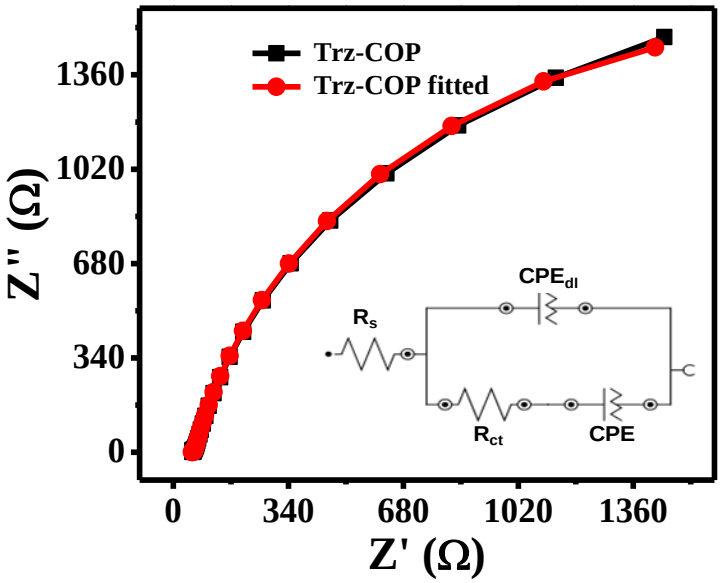

Figure S10. Electrochemical impedance spectroscopy (EIS) analysis of Trz-COP catalysts Nyquist plot, fitted plot and equivalent circuit.

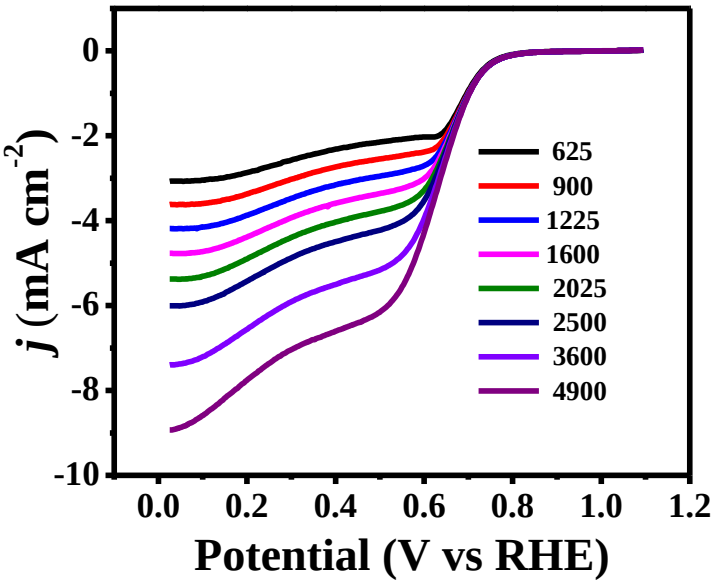

Figure S11. Linear sweep voltammetry (LSV) polarization curve of Trz-COP catalyst at all rotation speeds 625 to 4900 rpm in O_2 saturated 0.1 M KOH electrolyte solution

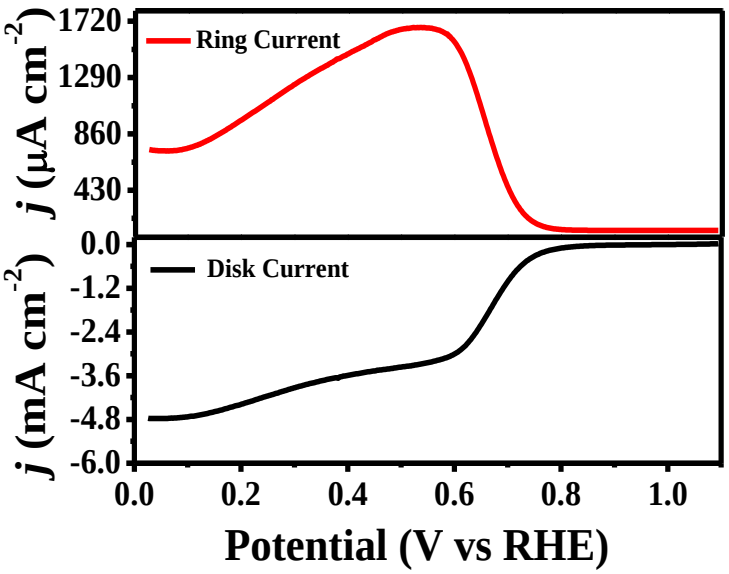

Figure S12. Linear sweep voltammetry (LSV) polarization curve of Trz-COP catalyst at 1600 rpm in O_2 saturated 0.1 M KOH electrolyte solution with disk and ring current.

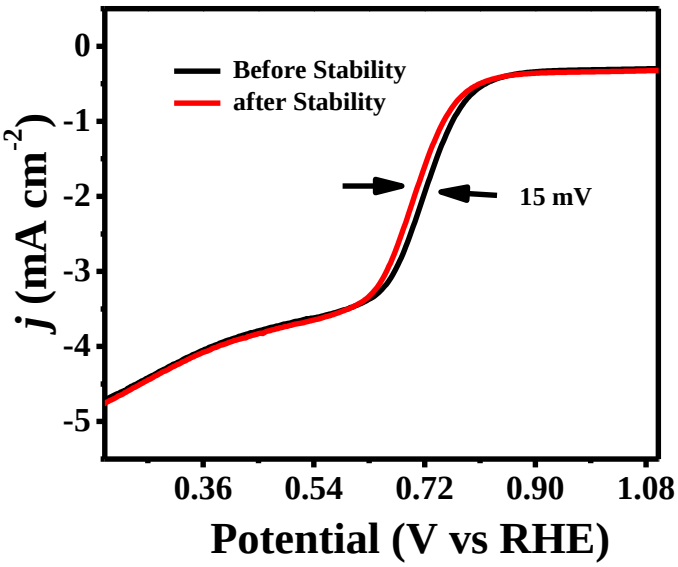

Figure S13. Linear sweep voltammetry polarization curve before and after stability of Trz-COP catalyst.

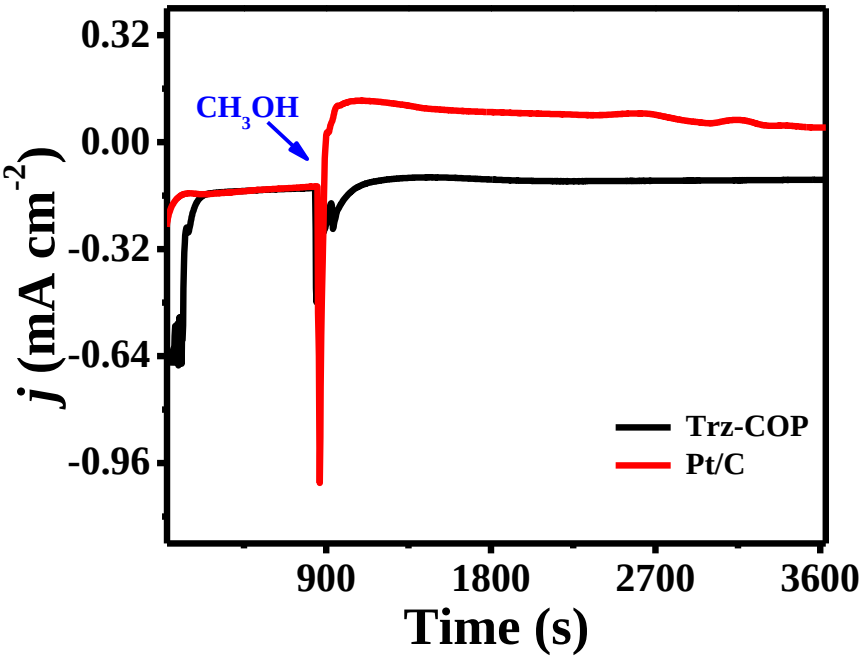

Figure S14. Chronoamperometry analysis of Trz-COP and Pt/C catalyst with 1M CH_3OH for checking methanol tolerance.

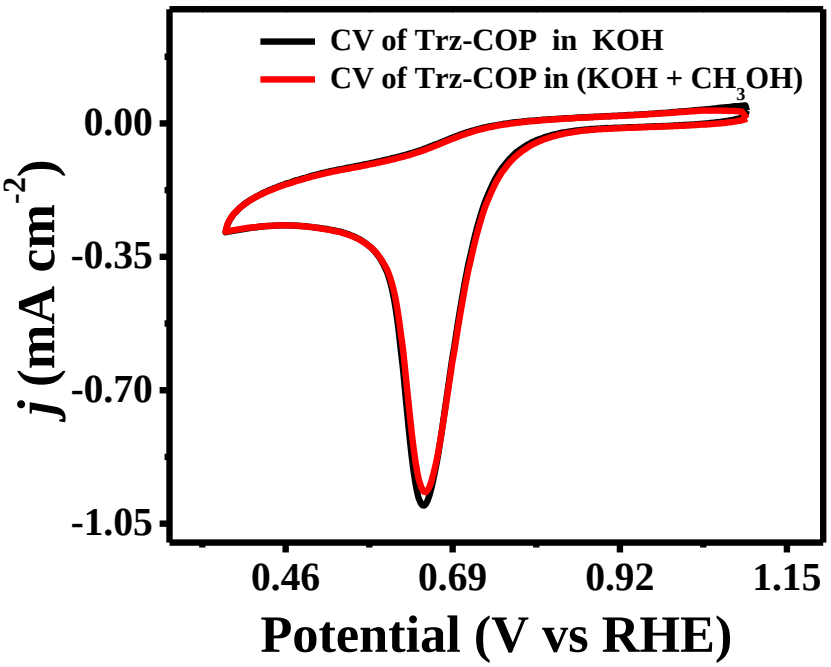

Figure S15. CV analysis Trz-COP catalyst with 1M CH_3OH and without CH_3OH in O_2 saturated KOH electrolyte.

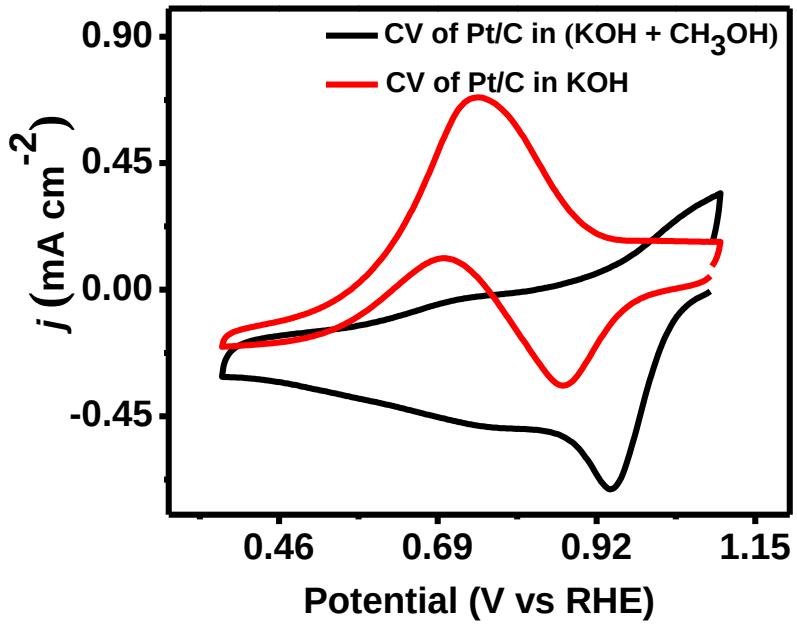

Figure S16. CV analysis of Pt/C catalyst with 1M CH_3OH and without CH_3OH in O_2 saturated KOH

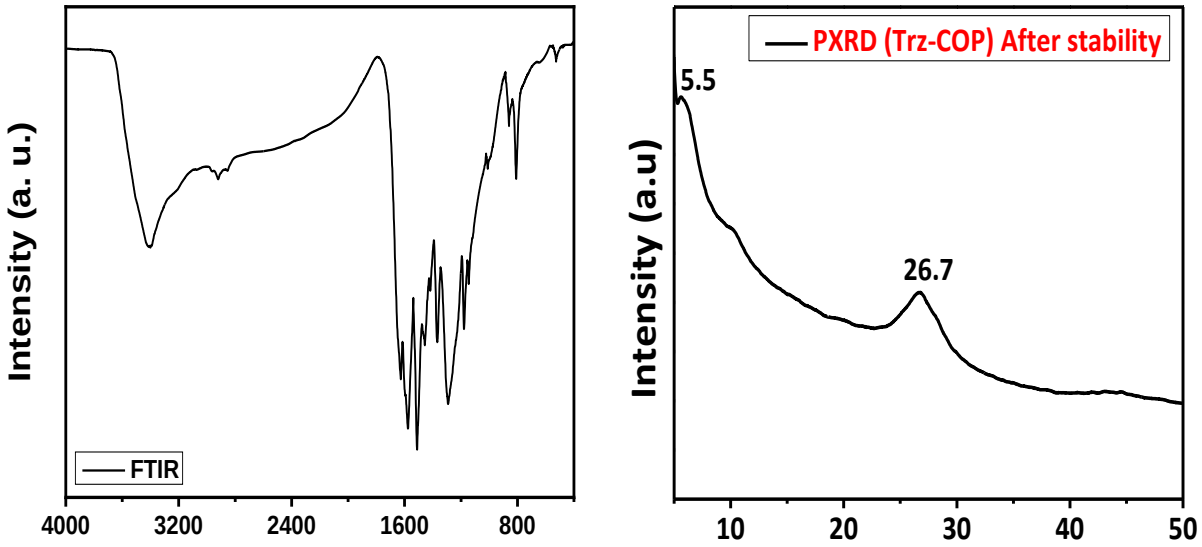

Figure S17. (a) FTIR (b) PXRD spectra of Trz-COP after stability

Section S2.

DFT study

Results and discussion

Figure S18, shows various 1:1 complex of O_2 and Trz-COP (A1, A2) optimized at the B3LYP/6-31+G (D, P) level of theory. The detailed methodology of obtaining such optimized complexes is described in detail in the Section S3. The zero-point vibrational energy (ZPVE) corrected complexation energy (ΔE_{Comp}^{ZPVE}) of these complexes, along with the bond length as well as bond elongation of the adsorbed O_2 molecule ($r_{O=O}$), are presented in **Table S4**. The complexation energy of A1 (-5.24 Kcal mol^{-1}) is higher than that of A2 (-1.87 Kcal mol^{-1}), which suggests that adsorption of O_2 at the imine site is preferred over the triazine containing site. Bond elongation value of adsorbed O_2 molecule for the imine and triazine site are 0.031 Å and 0.014 Å which indicates the catalytic activity towards ORR is also followed the same sequence respectively (imine site > triazine site). However, the dual active sites containing catalyst interact with O_2 molecules during the catalytic reaction through the favourable orientation of the C and N atoms.

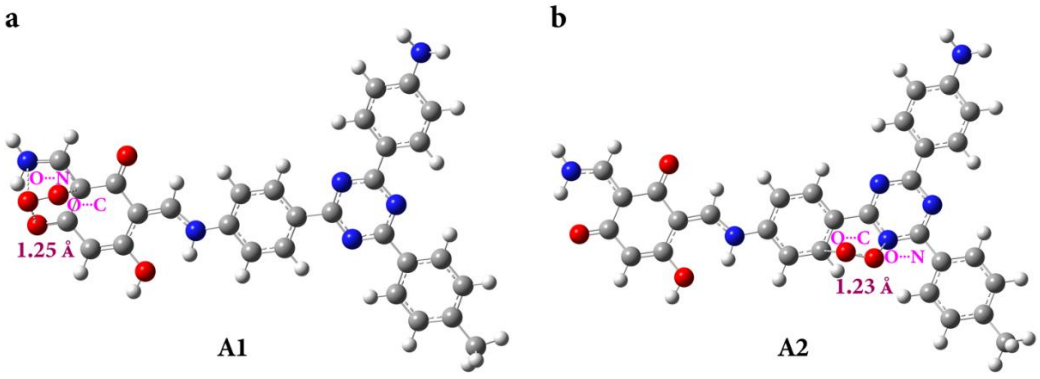

Figure S18. 1:1 complex of Trz-COP with dual binding sites interact with O_2, optimized at B3LYP/6-31+G (D,P) level of theory. The bond length of the adsorbed O_2 is mentioned in Å for each complex showing that O_2 bond length in these complexes has increased compared to that of the pure O_2.

Table S4. The zero-point vibrational energy (ZPVE) corrected complexation energy, O=O bond length (Å), type of the noncovalent interaction, electrostatic potential-derived atomic charges (a.u.), electron density [ρ(r)], Laplacian of electron density [L(r)] and ellipticity (ε) at the (3, -1)

bond critical point representing the respective noncovalent interaction of various 1:1 complex of Trz-COP form with O_2.

(1:1) Complex	ΔE_{Comp}^{ZPVE} (kcal.mol^{-1})	$r_{O=O}$ (Å)	Noncovalent interaction	ESP atomic charge (a.u.)	ρ(r) /a.u.	L(r) /a.u.	ε
A1	-5.24	1.246 (+0.031)	$(O_2)O\cdots C$	-0.060, -0.546	0.033	0.101	0.62
			$(O_2)O\cdots N$	-0.156, -0.909	0.012	0.036	0.45
			$(O_2)O\cdots O$	-0.156, -0.653	0.007	0.025	0.45
A2	-1.87	1.229 (+0.014)	$(O_2)O\cdots N$	-0.084, +0.073	0.009	0.028	1.19
			$(O_2)O\cdots O$	-0.03, -0.858	0.020	0.067	0.22
			$(O_2)O\cdots C$	-0.076, -0.094	0.026	0.076	0.36
			$(O_2)O\cdots N$	-0.040, -0.820	0.019	0.064	0.22

Next, atoms in molecules (AIM) analysis based on topological analysis of electron density was performed for all the optimized structures to unravel the type of interaction between the adsorbed O_2 molecule and Trz-COP moieties form. The electron density map of all the optimized complexes is shown in the supplementary materials along with the detailed methodology. The topological parameters of electron density, i.e., electron density [ρ(r)], Laplacian of electron density [L(r)], and ellipticity (ε) at the (3, -1) bond critical point (BCP) representing the respective noncovalent interaction of A1, and A2 listed in Table T2. Charge distribution and AIM analysis (Figure S19 and S20) show that the Trz-COP moiety adsorbs the O_2 molecule by weak noncovalent type interactions where anisotropy of electron density at the BCP can vary substantially based on the mode of interaction, suggesting a significant change in π/σ-bond character.

Section S3.

DFT experimental

Methodology. All the electronic structure calculations of the different 1:1 complexes of Trz-COP and O_2 where O_2 was attached to various bonding sites of Trz-COP and its tautomeric form were carried out at the B3LYP/6-31+G(D, P) level of theory using Gaussian 16 quantum chemistry program. The frozen core approximation and tight convergence criteria were employed in the optimization. The harmonic frequency calculations were performed for all the optimized structures to ensure that all the structures were at local minima. The electrostatic potential-derived atomic charges (ESP) were calculated using the MerzKollman algorithm. The zero-point vibrational energy (ZPVE) corrected complexation energy was calculated according to the following equation.

$$\Delta E_{Comp}^{ZPVE} = E_{Comp}^{ZPVE} - E_{TrzDFP}^{ZPVE} - E_{O_2}^{ZPVE} \quad \text{(S1)}$$

Next, AIM analysis[4–13] based on the topological analysis of electron density was performed on the optimized wavefunction of the (1:1) complexes of Trz-COP and O_2. A molecular density map was generated for all the complexes using AIM2000 software.[14] The electron density (ρ) and Laplacian of electron density [$\nabla^2\rho(r)$, L(r)] at each critical point connecting two nuclei known as a bond critical point (BCP) were computed. The presence of a (3, -1) type bond critical point (BCP) in which curvature of electron density at the BCP in the direction of the line connecting two nuclei participated in the bonding is positive, whereas the curvature in the two perpendicular directions to the bond path is negative confirms the nonbonding interaction between two nuclei. However, only those BCPs have been considered for the noncovalent interaction where ρ(r) and L(r) values are higher than 0.002 and 0.02 a.u., respectively.[12] Furthermore, the bond ellipticity (ε) at the BCP was also calculated according to the equation (S2), which measures the anisotropy of electron density at the BCP and can reflect the π or σ-bond character of a chemical interaction between two nuclei.

$$\varepsilon = \frac{\lambda_1}{\lambda_2} - 1 \quad \text{(S2)}$$

Where, λ 's are the negative vectors associated with the hessian of ρ at that CP and $\lambda_2 \leq \lambda_1$. Greater the value of ε more is the accumulation of electron density at the perpendicular axes at the BCP along the bond path connecting two nuclei; more is the π-bond character.

Electrostatic potential-derived atomic charges of the 1:1 optimized complex of Trz-COP and O_2

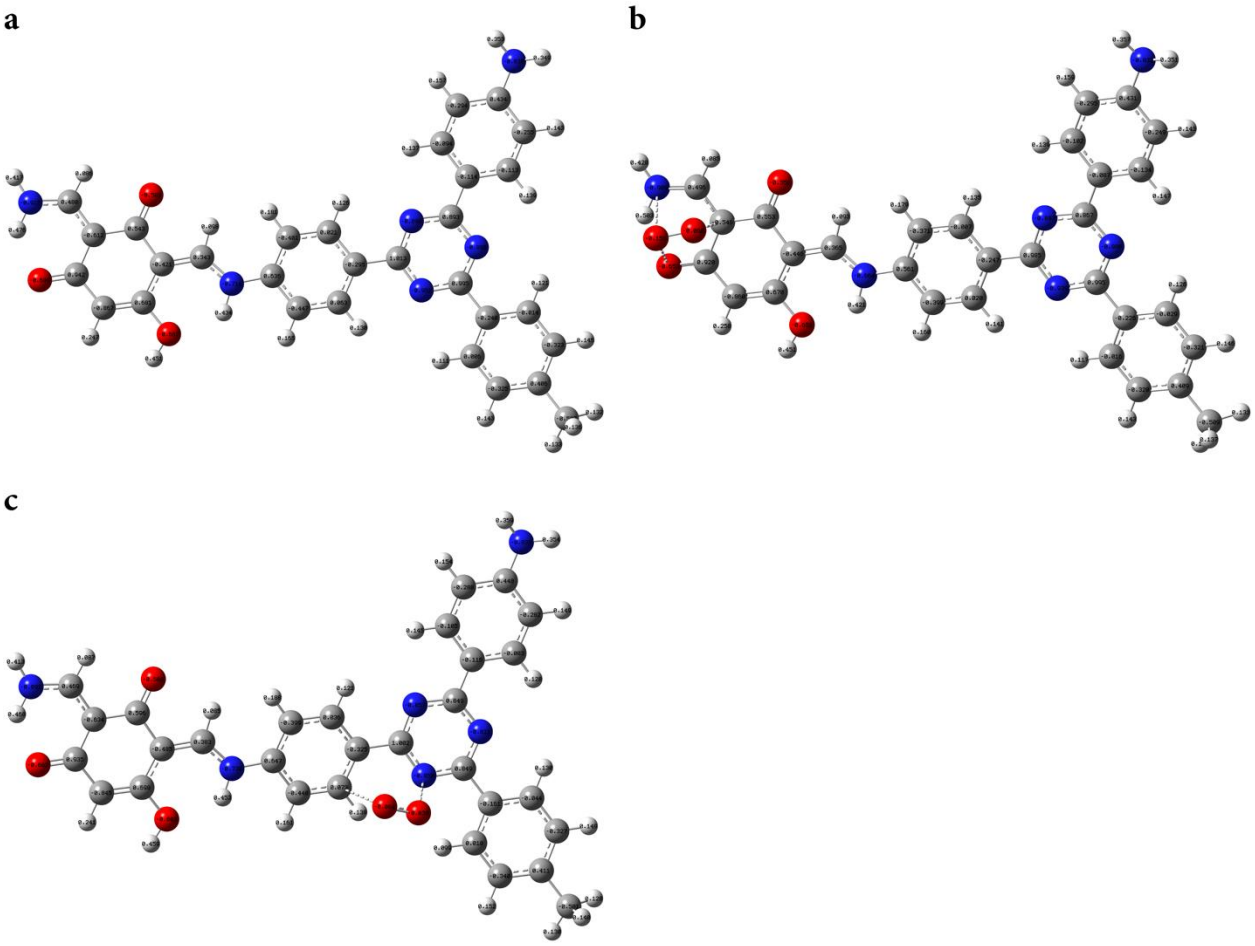

Figure S19. ESP-derived atomic charges of (a) Trz-COP and its 1:1 complex with O_2, (b) A1, and (c) A2.

Electron density map of the 1:1 optimized complexes of Trz-COP and O_2 estimated at B3LYP/6-31+G(D, P) level of theory

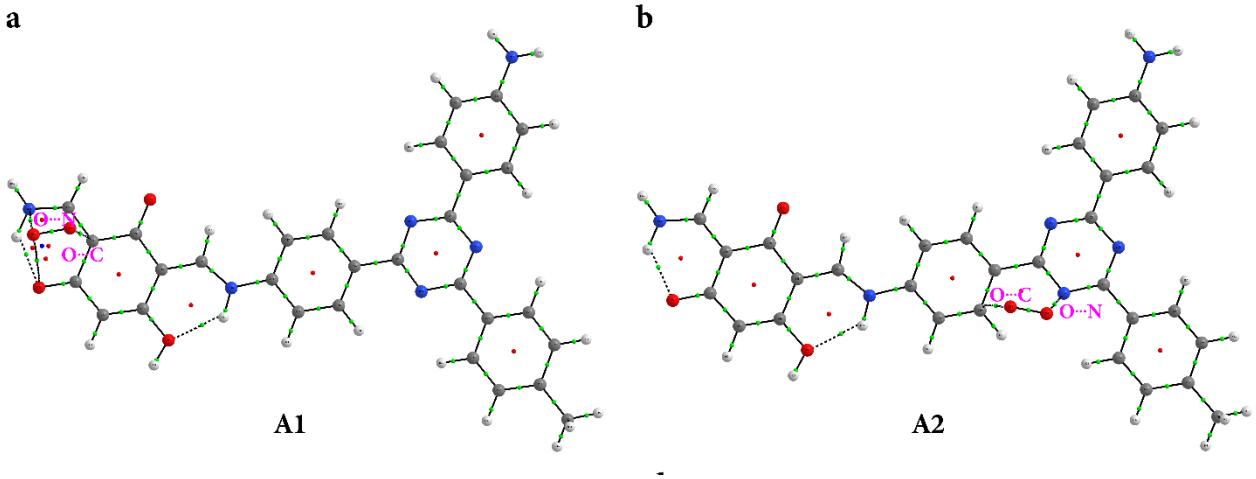

Figure S20. Molecular electron density map of the 1:1 complexes of O_2 with Trz-COP (A1, A2) calculated at B3LYP/6-31+G(D,P) level of theory. Green and red spheres represent bond critical points (BCP) and ring critical points (RCP). The presence of BCP between the phenyl ring carbon along with nitrogen atom (from -C-N of imine and triazine) and O_2 molecule as well as terminal

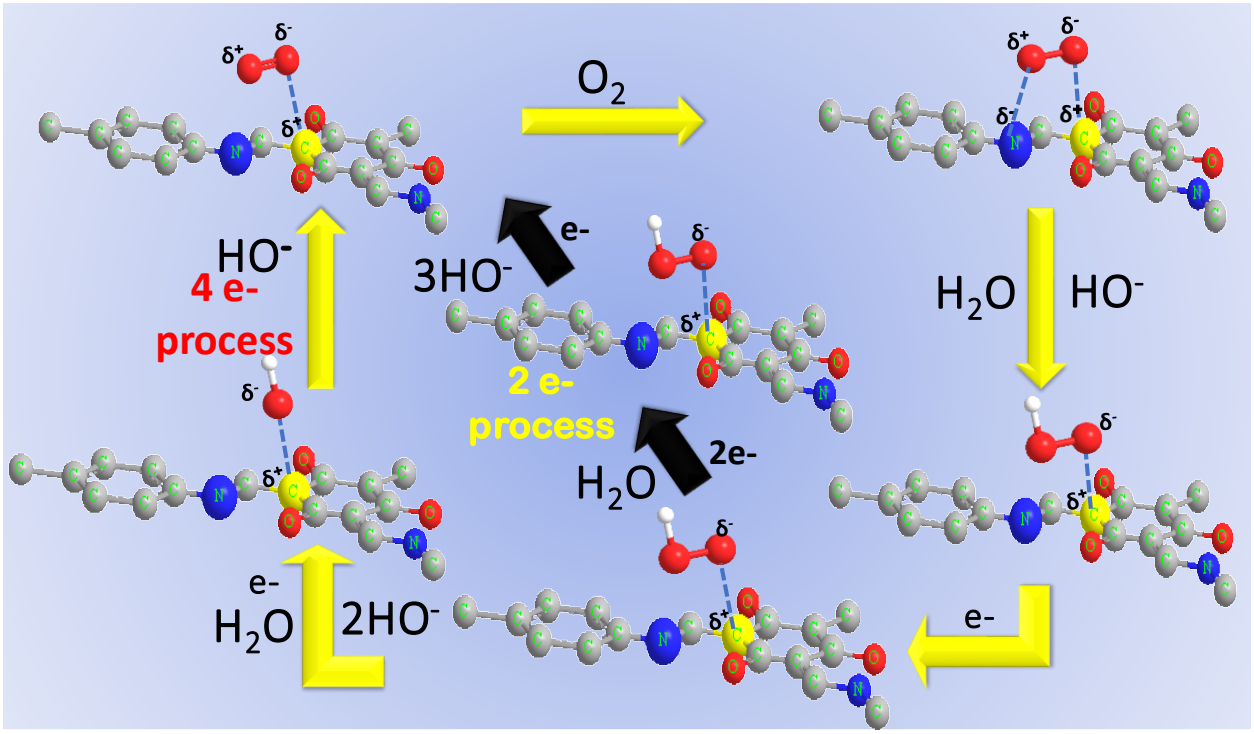

Figure S21. Mechanistic pathway for ORR

Supporting references

1 A. Modak, J. Mondal, V. K. Aswal and A. Bhaumik, *Journal of Materials Chemistry*, 2010, **20**, 8099–8106.

2 R. Gomes, P. Bhanja and A. Bhaumik, *Chemical Communications*, 2015, **51**, 10050–10053.

3 R. Zhou, Y. Zheng, M. Jaroniec and S.-Z. Qiao, *ACS Catalysis*, 2016, **6**, 4720–4728.

4 R. F. W. B. T.-A. in Q. C. Bader, Academic Press, 2009, vol. 57, pp. 285–318.

5 R. F. W. Bader, *The Journal of Physical Chemistry A*, 2009, **113**, 10391–10396.

6 V. Tognetti and L. Joubert, *Physical Chemistry Chemical Physics*, 2014, **16**, 14539–14550.

7 C. F. Matta and R. F. W. Bader, *The Journal of Physical Chemistry A*, 2006, **110**, 6365–6371.

8 R. F. W. Bader, *Chemistry (Weinheim an der Bergstrasse, Germany)*, 2006, 12, 7764–7769.

9 R. F. W. Bader and D.-C. Fang, *Journal of Chemical Theory and Computation*, 2005, **1**, 403–414.

10 J. Hernández-Trujillo and R. F. W. Bader, *The Journal of Physical Chemistry A*, 2000, **104**, 1779–1794.

11 R. F. W. Bader and D. Bayles, *The Journal of Physical Chemistry A*, 2000, **104**, 5579–5589.

12 U. Koch, *The journal of physical chemistry.*, 99, 9747–9754.

13 R. F. W. Bader, *Chemical Reviews*, 1991, **91**, 893–928.

14 file:///C:/Users/Sabuj K. D. 6b0158. (1).ris, *Journal of Computational Chemistry*, 2001, **22**, 545–559.